

Theory and Experiments on Multi-Ion Permeation and Selectivity in the NaChBac Ion Channel

W. A. T. Gibby^{*†}, M. L. Barabash^{*}, C. Guardiani^{*}, D. G. Luchinsky^{**†},
O. A. Fedorenko^{‡§}, S. K. Roberts[‡] and P. V. E. McClintock^{*}

^{*}Department of Physics, Lancaster University
Lancaster LA1 4YB, UK

[†]SGT, Inc., Greenbelt, MD, 20770, USA

[‡]Division of Biomedical and Life Sciences
Lancaster University
Lancaster, LA1 4YG, UK

[§]School of Life Sciences, University of Nottingham
Nottingham, NG7 2UH, UK

[†]w.gibby@lancaster.ac.uk

Received 1 November 2018

Accepted 7 February 2019

Published 1 April 2019

Communicated by Igor Khovanov

The highly selective permeation of ions through biological ion channels is an unsolved problem of noise and fluctuations. In this paper, we motivate and introduce a non-equilibrium and self-consistent multi-species kinetic model, with the express aims of comparing with experimental recordings of current versus voltage and concentration and extracting important permeation parameters. For self-consistency, the behavior of the model at the two-state, i.e., selective limit in linear response, must agree with recent results derived from an equilibrium statistical theory. The kinetic model provides a good fit to data, including the key result of an *anomalous mole fraction effect*.

Keywords: Ion channel; anomalous mole fraction effect; NaChBac; kinetic theory.

1. Introduction

Biological ion channels passively (and stochastically) transport ions through the impermeable cell membrane, but precisely how they do it is a long-standing problem [1–3]. Many families of channels exist which can be further subcategorized by their primary conducting ions and gating mechanisms. In this work, we shall focus on a

This is an Open Access article published by World Scientific Publishing Company. It is distributed under the terms of the Creative Commons Attribution 4.0 (CC-BY) License. Further distribution of this work is permitted, provided the original work is properly cited.

W. A. T. Gibby *et al.*

family of narrow voltage-gated channels [4]; and in particular on the prokaryotic Na^+ channel NaChBac, from *Bacillus halodurans* [5]. This represents a model channel providing insight into mammalian voltage-gated channels which play an important role in numerous physiological processes, for example the propagation of the action potential; and have many interesting permeation properties such as high selectivity and blocking phenomena [1–3].

The Anomalous Mole Fraction Effect (AMFE) is a good demonstration of blocking in multi-ion pores. A typical experiment involves considering a pair of conducting species, where one bulk solution is held constant while the ionic concentrations are varied in the other bulk solution. The outcome is a reduction in conductance of the mixed ionic solutions versus pure solutions [6]. It is generally assumed that these channels must conduct ions in single-file through multiple binding sites; however, AMFE has also been observed in simulations involving a single site [7]. AMFE can be observed in many channels, including but not limited to: K^+ and Ca^{++} channels [2, 8–10] and NaChBac [11].

Prokaryotic channels are an attractive choice because they exist in a simpler protein structure whilst maintaining the permeation properties of their eukaryotic counterparts. The first prokaryotic voltage-gated Na^+ channel identified, was NaChBac in 2001 [5]. A crystal structure is not yet available, but homology models of suggested structure exist (see Fig. 1) [12, 13]. These suggest four main binding sites, with two sites playing the dominant role and a knock-on conduction mechanism for Na^+ . The selectivity filter (pore) has a length $L_c = 14 \text{ \AA}$ and average radius $R_c = 2.8 \text{ \AA}$; geometrically constraining the pore to 4 or 6 K^+ or Na^+ ions in single file, respectively. The two dominant sites are located at the level of the carbonyl oxygen

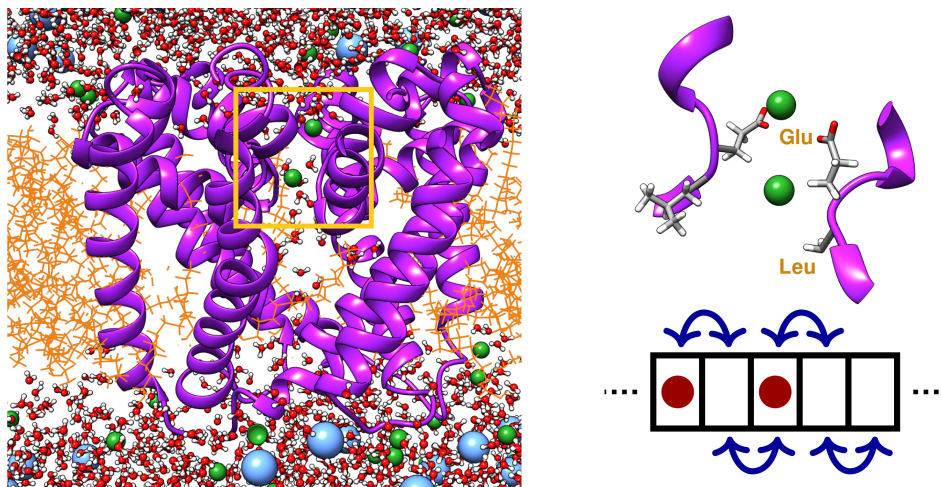


Fig. 1. **Left**, structure of NaChBac [12], made using Chimera [14]. The protein (purple ribbons) is embedded into a lipid membrane (orange lines) and solvated on either side by a NaCl solution (blue and green spheres). **Right** and top, zoomed in view of the selectivity filter representing the pore (highlighted by the yellow box) and right bottom, the lattice approximation of the pore.

groups provided by the leucine residues (site 1) and the charged glutamate ring (site 2). The first site has a diameter $\sim 5.5 \text{ \AA}$ and therefore is wide enough to accommodate the full primary hydration shell of a transiting Na^+ ion. Thus, Na^+ is prevented from interacting directly with the dipolar charge from the oxygen atoms. Site 2 is narrower with a diameter of $\sim 5 \text{ \AA}$; and therefore, the Na^+ ion suffers partial dehydration of its first shell. This energetic cost is offset by direct interaction with the glutamates. In each case, the depth of the free energy well is almost identical.

A common approach to modeling such stochastic systems involves Eyring rate or kinetic theory. One generally assumes that the pore can be represented by a series of energy wells and barriers, and that occupancies (or states) can be described by a set of master equations from which the net flux can be calculated. Typically these reproduce saturation of current versus concentration, as observed experimentally [15–17], but also more interesting properties such as: the importance of volume exclusion [18], the role of selectivity and interactions between ions [16, 19, 20] and the consequence of mutagenesis [21]. Generally, this approach faces a persistent criticism over the validity of the transition rates [22–24], their relation to structure [25] and self-consistent inclusion of concentration into the energy barrier [26]. To counter this, efforts have been made to define rates rigorously using mean first passage time (mfpt) theory [26, 27] or equilibrium statistical theory [28].

In this paper, we aim to overcome these issues by developing a multi-species kinetic model within the theoretical framework introduced in earlier work [29, 30]. We have the explicit aims of validating the theory by comparison with experimental recordings for NaChBac including the blocking phenomena AMFE, and of explicitly calculating useful parameters including the energy barriers at each binding site and the effective diffusion coefficient in the pore. We start by defining the total system, the state space, the corresponding energy spectra and the statistical ensemble. The statistical fluctuations are then related directly to the flow of ions at linear response. The model is then extended far from equilibrium by a set of master equations where the transition rates are defined by comparison of the linear responses with equilibrium behavior.

In the work that follows, with SI units: q, k, T , respectively, represent the proton charge, Boltzmann’s constant and the system temperature. We use the following bulk diffusion coefficients: $D_{\text{K}}^b = 1.96 \times 10^{-9} \text{ m}^2 \text{ s}^{-1}$ and $D_{\text{Na}}^b = 1.33 \times 10^{-9} \text{ m}^2 \text{ s}^{-1}$, for K^+ and Na^+ , respectively.

2. Theoretical Approach

2.1. Discrete system

To define the system let us consider a pore, thermally and diffusively coupled on either side to bulk reservoirs [29]. Under typical experimental or physiological conditions the thermal de Broglie wavelength Λ of e.g., the ion Na^+ has $\Lambda \sim 20 \text{ pm}$. We note that this is much less than the average distance between ions in the bulk and

W. A. T. Gibby et al.

even in narrow pores. Hence to a reasonable approximation the system is classical, and therefore the ions obey Boltzmann statistics. The physical properties of the system are determined by the canonical ensemble assuming constant total volume V and temperature T , and conservation of the total number of particles N_i of each species i . However, we note that, in general, the van der Waals forces (that are of quantum origin) still play a fundamental role in ionic permeation and these will be included in future work. We approximate the ion channel as the selectivity filter, which we treat as a 1D lattice (see Fig. 1) with a total of M binding sites. Each site in the lattice can hold at most 1 ion and the bulk reservoirs contain mixed solutions of arbitrary concentration. Since the lattice has a finite number of sites, its occupancy represents a state of the system, and the total set of states is denoted by $\{n_j\}$. Each state is then characterized by the set of occupation numbers, for each species $i \in 1, \dots, S$ at all individual sites $m \in 1, \dots, M$ labeled from left to right: $\{n_{im}\} = [n_{i1}, n_{i2}, \dots, n_{iM}]$ where $\sum_{i=1}^S n_{im} \in 0, 1$ and $\sum_{m=1}^M \sum_{i=1}^S n_{im} \leq M$.

2.2. Effective grand canonical ensemble

In earlier work [29, 30] we demonstrated that such a system can be formulated within the effective grand canonical ensemble, with the following Gibbs free energy,

$$G(\{n_j\}; n_f) = \mathcal{E}(\{n_j\}; n_f) + W(\{n_j\}) - \sum_{i=1}^S \sum_{m=1}^M n_{im} [\Delta \bar{\mu}_{im}^b + kT \ln(x_i^b)]. \quad (1)$$

Here, $\mathcal{E}(\{n_j\}; n_f)$ denotes the electrostatic contribution which includes the ion–ion and ion–pore long range interactions. The indistinguishability of ions and empty sites is included via $W(\{n_j\})$, which manifests via the natural logarithm of the factorial of total number of occupying ions $\sum_i n_i!$ and the factorial of the number of empty sites $n_{es}!$ (which is equal to $(M - \sum_i n_i)!$). The final term includes contributions from the excess chemical potential difference between the bulk and binding site $\Delta \bar{\mu}_{im}^b$, and the natural logarithm of the bulk mole fraction $x_i^b \sim c_i^b/c_W$. The excess chemical potential difference describes the difference in non-ideal local interactions between the pore and site, and is largely dominated by the dehydration energy of the ion [31, 32].

Within this ensemble (see [29, 30] for full details) we can calculate the current I and conductivity σ of the favored ion in the high selective limit, which is shown to be proportional to the variance in the particle number.

$$I_i = \sigma_i \nabla \mu_i \quad \text{and} \quad \sigma_i \propto kT \frac{\partial \langle n_i \rangle}{\partial \eta_i^c}. \quad (2)$$

Here, μ_i and η^c are the electro-chemical and chemical potentials in the pore.

2.3. Kinetic theory

To extend the theory far from equilibrium, we introduce a set of master equations describing transitions within our state space. Importantly, this approach requires the specification of transition rates Γ , which must be functions of the energy barrier to

enter/exit each state. We have seen that each site which can be occupied by at most one ion is described by a transition number n_m equal to the sum over all possible species i at the site. The total network can be written in matrix form $\dot{\mathbf{P}} = \mathbf{P}\Gamma$, with the row describing each state given by,

$$\begin{aligned} \dot{P}(\{n_1, \dots, n_m, \dots, n_M\}) = & \sum_{n_m^* = \left\{ \begin{array}{l} n_m + n_i^* \\ n_m - n_i^* \end{array} \right\}^{\star}} P(\{n_1, \dots, n_m^*, \dots, n_M\}) \Gamma_{n_m^*, n_m}^i \\ & - P(\{n_1, \dots, n_m, \dots, n_M\}) \Gamma_{n_m, n_m^*}^i. \end{aligned} \quad (3)$$

The right-hand side describes the transiting ion n_i^* , either entering the m th state, or exiting and entering one of the $m \pm 1$ states. For clarity, the conditions \star are imposed which require that the state of the pore must remain within the state space and the transitions be physically possible i.e., an ion can only enter a neighboring and empty site, and an ion can only exit from a site that it is already occupying. This set of equations is similar to those commonly used to describe electron flow in quantum structures [33, 34], with the important difference that here we do not allow transport into any empty site but instead specify via the conditions \star .

Since the time-scale of permeation is short ~ 10 ns, it is safe to neglect temporal behavior and consider $\dot{P} = 0$. The steady-state current can be defined for all possible transitions involving each binding site, where Kirchoff's laws are satisfied. Hence the current at each site can be defined from the balance of fluxes, such that its positivity defines ionic flow from left to right. Hence, the current into the m th site can be written as

$$\begin{aligned} I_i(\{n_j\}) = & q[P(n_1, \dots, n_{m-1}, n_m, 0, \dots, n_M) \Gamma_{n_m, n_m+1}^i \\ & - P(n_1, \dots, n_{m-1}, 0, 1, \dots, n_M) \Gamma_{n_m+1, n_m}^i], \end{aligned} \quad (4)$$

where we note that the total current can be calculated by summing over all possible states for transitions to the first site. In the equilibrium limit, the transition rates must be constrained by the condition of detailed balance; and the probabilities will reduce to the form given by equilibrium statistical physics [29, 30, 35].

3. Application to NaChBac and its Mutant

To describe the permeation of NaChBac and its mutant we employ a toy model with two binding sites; and the potential energy profiles shown in Fig. 2. Note that, in general, the depth of the well at either site does not have to be equivalent, and it may change depending on the state. Since anions are electrostatically repelled by the negative pore charge n_f , for two conducting species e.g., Na^+ and K^+ we have nine possible states. We label these $A - I$ for the purpose of notational clarity in Fig. 2 and Eqs. (5) and (6). We note that terms $\Delta\bar{\mu}_i^b$ depend on the species and hence result in energy level splitting (see Fig. 3).

$$\{00\}_A, \{X0\}_B, \{0X\}_C, \{Y0\}_D, \{0Y\}_E, \{XX\}_F, \{YY\}_G, \{XY\}_H, \{YX\}_I. \quad (5)$$

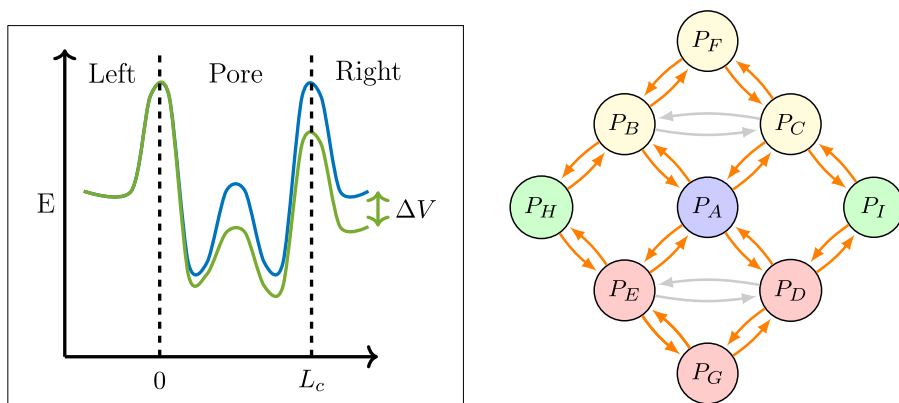


Fig. 2. (Color online) **Left**, potential energy profile where blue and green curves represent equilibrium between the bulks and the influence from an applied voltage ΔV . The voltage drops linearly across the pore $[0, L_c]$ and, in general the well depths may not be identical. **Right**, the discrete-state transition mechanism of the permeating ion. Red and yellow circles denote the pure K^+ and Na^+ states, and green and blue define the mixed and ground states. Arrows describe possible transitions, with orange involving one of the bulks and gray being internal.

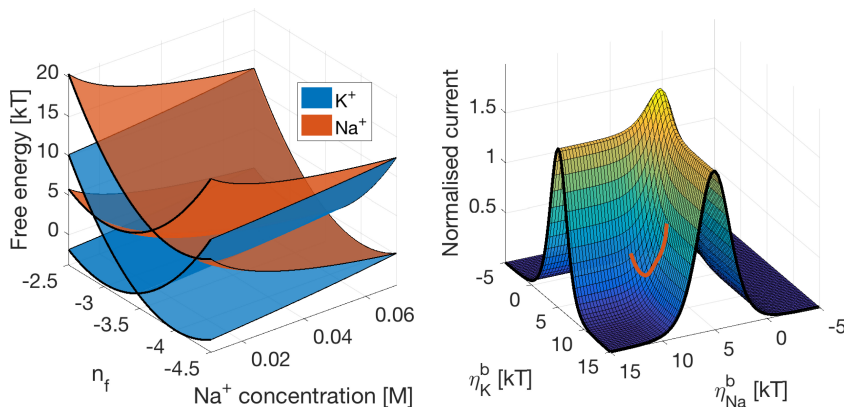


Fig. 3. **Left**, energy spectra of the pure 3 and 4 ion states versus filter charge n_f and Na^+ concentration. To agree with the experimental conditions the concentrations of the two species always sum to 0.14 M and hence: $x_K = (0.14/c_W - x_{Na})$. The excess chemical difference is taken to be 0 with $\Delta\bar{\mu}_K = \Delta\bar{\mu}_{Na} = 1 kT$, and as such the filter is only selective based on the concentration. Along the n_f plane levels are parabolic, minimizing when $n_f = \sum_i n_i$. At low Na^+ concentrations Na^+ faces a large concentration energy barrier with its barrier-less transition (the crossing of neighboring levels) occurring at a larger free energy point. As Na^+ concentration increases the levels converge in the absence of selectivity, and start to invert beyond this point with Na^+ now becoming favored. **Right**, normalized Na^+ and K^+ conduction peaks for adding a single ion to an empty pore versus the concentration dependent chemical potential $\eta_i = kT \ln(x_i) + \bar{\mu}_i$ assuming that $D_i^c = 5 \cdot 10^{-10} m^2 s^{-1}$, $E_T^b = 0.5 kT$, $\Delta E_{T,i}^c = 0.5 kT$ and $\Delta\mathcal{E} + \bar{\mu}_{im}^c = -5 kT$. In the selective regions $|\Delta\eta_K - \Delta\eta_{Na}| \gg 0$ species specific conduction peaks are observed, maximizing under the conditions $\Delta G \sim 0$. Away from these peaks *ionic Coulomb blockade* occurs and the current is zero [11, 29, 34, 39]. The blocking effect AMFE can be observed qualitatively: the orange curve represents the experimental data points.

The corresponding set of master equations can be written as

$$\dot{\mathbf{P}} = \begin{pmatrix} -\mathcal{M}_A & \Gamma_{BA} & \Gamma_{CA} & \Gamma_{DA} & \Gamma_{EA} & 0 & 0 & 0 & 0 \\ \Gamma_{AB} & -\mathcal{M}_B & \Gamma_{CB} & 0 & 0 & \Gamma_{FB} & 0 & \Gamma_{HB} & 0 \\ \Gamma_{AC} & \Gamma_{BC} & -\mathcal{M}_C & 0 & 0 & \Gamma_{FC} & 0 & 0 & \Gamma_{IC} \\ \Gamma_{AD} & 0 & 0 & -\mathcal{M}_D & \Gamma_{ED} & 0 & \Gamma_{GD} & 0 & \Gamma_{ID} \\ \Gamma_{AE} & 0 & 0 & \Gamma_{DE} & -\mathcal{M}_E & 0 & \Gamma_{GE} & \Gamma_{HE} & 0 \\ 0 & \Gamma_{BF} & \Gamma_{CF} & 0 & 0 & -\mathcal{M}_F & 0 & 0 & 0 \\ 0 & 0 & 0 & \Gamma_{DG} & \Gamma_{EG} & 0 & -\mathcal{M}_G & 0 & 0 \\ 0 & \Gamma_{BH} & 0 & 0 & \Gamma_{EH} & 0 & 0 & -\mathcal{M}_H & 0 \\ 0 & 0 & \Gamma_{CI} & \Gamma_{DI} & 0 & 0 & 0 & 0 & -\mathcal{M}_I \end{pmatrix} \begin{pmatrix} P_A \\ P_B \\ P_C \\ P_D \\ P_E \\ P_F \\ P_G \\ P_H \\ P_I \end{pmatrix}. \quad (6)$$

Here, the rates Γ are defined such that the superscript defines the order of transitions between states i.e., Γ_{AB} implies transitions between states A and B (see (5)). Diagonal matrix elements are equal to the sum over all transitions involving the site, and the columns sum to zero; and thus we can replace one row with probability conservation. There are two transition types: (i) external i.e., involving a bulk and (ii) internal i.e., between sites. Before we discuss the general form of the rates we note two important properties. In perfectly planar and neutral membranes the transmembrane potential is linear across the pore [32, 35], illustrated by the green line in Fig. 2. For simplicity, we shall define it as follows by taking $\phi^L = \phi$, $\phi_m^c = \chi_m \phi$ and $\phi^R = 0$, where χ_m describes the relative position of the site m . Consequently, only the exiting rate is influenced by the work done in moving against this potential. From the condition of detailed balance we can define each rate using a functional normalization, which will be computed by comparison of the linear response with Eq. (2),

$$\Gamma_{m,i}^{\text{In},b} = x_i^b A^{b,i} e^{-E_{T,i}^b/kT}, \quad (7)$$

$$\Gamma_{m,i}^{\text{Out},b} = A^{b,i} e^{-(E_{T,i}^b + \Delta G_{im}^B + qz_i(\phi^b - \chi_m \phi))/kT}, \quad (8)$$

$$\Gamma_{m_T, m_F}^i = B^i e^{-(\Delta E_{T,im}^c + qz_i \phi(\chi_{i_T}^c - \chi_{m_T})) / kT}. \quad (9)$$

The terms with subscript T represent the contributions from the transition states. We shall consider that the transition state barriers at the bulk-pore interface $E_{T,i}^b$ are identical at either entrance and for both species, although in general this may not be the case. We also introduce the parameter ΔG_{im}^B to represent the binding energy at each site,

$$\Delta G_{im}^B = kT \ln \left(\frac{n_{es}}{n_i + 1} \right) + \Delta \bar{\mu}_{im} - \Delta \mathcal{E}, \quad (10)$$

where the terms are as defined in Eq. (1). The internal barrier $\Delta E_{T,im}^c$ is given by the difference between the internal transition state level and the local interaction at each site: $\Delta E_{T,im}^c = E_{T,i} - \bar{\mu}_{im}^c$.

To calculate these normalizations A/B , we reduce the system to two-states i.e., a single-site. We thus eliminate internal transitions and apply the condition of

selectivity such that we consider each species separately. By comparison of the linear response, we find that the normalization of A must take the form

$$A^{b,i} = \frac{D_i^c}{L_c^2} \frac{2}{x_i^b + e^{-\Delta G_{im}^B/kT}}, \quad (11)$$

where ΔG_{im}^B describing each site is given by (10). For symmetrical solutions these normalizations are identical at either bulk and reduce to a suppressing (Kramer's type) exponential function in the limit $|\Delta G| \gg 0$. We allow these normalizations to differ for asymmetrical solutions (without including the Nernst potential), yet it still reproduces the Kramer's limit if the local energy barrier ΔG_{im}^B becomes large. This form is similar to the creation/annihilation probabilities used within the grand canonical Monte Carlo formalism [32, 36]. To maintain units and convention we shall also introduce the internal normalization $B^i = D_i^c/L_c^2$.

3.1. Comparison with experiment

To compare the theory with experimental recordings and make predictions we consider two experiments. For further details of the experimental methods, including generation of mutant channels and their expression, as well as details of electrophysiological experiments, we refer to [11], and here we only present a concise summary. In the first series of experiments we performed whole-cell current measurements through a NaChBac mutant (LDDWAD) channel, which we assume to have the same conduction mechanism as wild type NaChBac, in different Na^+/K^+ concentrations (AMFE experiment). In these recordings the pipette solution contained (in mM) 15 Na-gluconate, 5 NaCl, 90 NMDG, 10 EGTA, and 20 HEPES, pH 7.4 (adjusted with 3mM HCl), meanwhile the bath solution contained (in mM); 137 NaCl, 10 HEPES and 10 glucose, pH 7.4 (adjusted with 3.6 mM NaOH). Permeability to K^+ was investigated by replacing the NaCl bath solution with an equivalent KCl solution such that the total ionic concentration was fixed at 140 mM. Total current across the cell was then normalized and, because one can assume that the total number of channels and their type is conserved in each cell for the duration of the recording, it can effectively be modeled as a single channel. Data were collected and the peak current magnitude in the current–voltage relationship was found at a -25 mV voltage drop across the channel. Consequently, there exists strong electrochemical gradients on the ions particularly when Na^+ concentration exceeds 0.07 M (the magnitude of the gradient exceeds $2kT$); and when there is an absence of ions in one side of the membrane e.g., when the bath solution is devoid of Na^+ . The second experimental comparison is with single-channel NaChBac channel recordings using an identical bath and pipette solution containing (in mM: 137 NaCl, 10 HEPES and 10 glucose, pH 7.4 adjusted with 3.6 mM NaOH). Single-channel recordings are possible because Na^+ is the preferred substrate with sufficiently high conductance as to provide a single-channel current amplitude which significantly exceeded noise (i.e., a favorable signal to noise ratio).

3.2. Linear response

To investigate the permeation process we shall consider the behavior of the kinetic equations under close-to-equilibrium conditions i.e., the linear response. The bulk solutions are considered symmetrical and take the form given by the bath solution in the experiment with a small voltage drop equivalent to $1 kT$ is applied.

In Fig. 3 (left), we consider the energy spectra of the pure states only in the system versus filter charge n_f and Na^+ concentration where the K^+ concentration is given by $c_K = 0.14M - c_{\text{Na}}$. We also note that the binding interactions of the species are taken to be the same. The electrostatic interaction \mathcal{E} is taken from [37, 38], and is equal to $U_c \cdot (\sum_i n_i + n_f)^2$, where U_c is the charging energy. We note that for the NaChBac geometry it is relatively small and takes the value $\sim 6 kT$. In the n_f plane, the energy spectra form a series of parabolic curves, arranged according to ionic species and number of ions in the pore. The energy spectra can cross at particular values of n_f , where the energy difference is barrierless $\Delta G \sim 0$. This corresponds to degeneracies in the state of the pore and results in resonant conduction of the favored ion (see Fig. 3); the disfavored ion faces an energy barrier which prohibits conduction. This corresponds to Eisenmann selectivity [29, 30], and in this example it reduces to the difference in concentrations of the species. As the Na^+ concentration increases, the selectivity barrier becomes smaller until 0.07 M and then changes sign. Consequently, the free energy spectra of the pure Na^+ states become less than their K^+ counterparts and the pore now favors Na^+ .

Figure 3 (right) displays the normalized conduction of the pore in the linear response regime with a small voltage gradient of 25 mV, and the condition of an identical diffusion rate in the pore. It is plotted versus the chemical potentials of both species $\eta_i = kT \log(x_i) + \bar{\mu}_i^b$; and only considers the transition from 0 to 1 ions in the filter. We observe a conduction peak, forming in the selective limits for either species. Peaks maximize under the condition that $\Delta G \sim 0$ i.e., a barrierless transition which is governed by *ionic Coulomb blockade* [11, 29, 34, 39]. The orange curve represents the experimental data from LDDWAD exhibiting the blocking effect AMFE. For clarity these are placed on the conduction peak. The qualitative agreement proves that the intersection of the two curves can reproduce this blocking effect. To improve agreement we would clearly need to fit the data under non-equilibrium conditions and this will be undertaken in Sec. 3.3.

3.3. Non-equilibrium response

In order to compare with the experimental results we shall now use the kinetic model, implementing the exact experimental conditions. To reduce the fitting parameters we shall introduce $\chi_1 = 0.66$, $\chi_2 = 0.33$ and $\chi_T^c = 0.5$, and constant bulk-pore transition state barriers of 1 and $0.5 kT$ in the NaChBac and AMFE comparison, respectively. The free parameters are the binding energy at each site $\Delta G_{im}^{B,b}$, the internal energy barrier $\Delta E_{T,im}^c$ and the parameter α . This is introduced via the relation $D_i^c = \alpha D_i^b$ and necessary because unlike in the bulk, the diffusivity in the

W. A. T. Gibby et al.

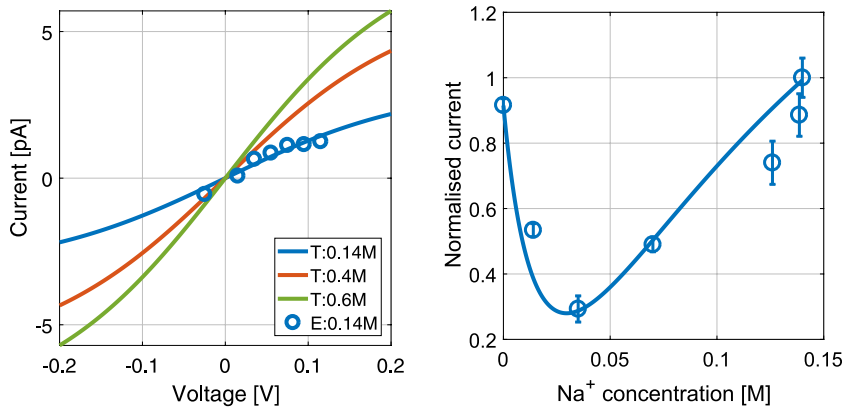


Fig. 4. **Left**, theoretical (T) current fitted against single-channel experimental recordings (E) for NaChBac using the following fitting parameters: $\alpha = 0.5$, for the first and second ions entering the pore respectively (in kT): $\Delta G_{\text{Na}}^B = 3.75$ and $\Delta G_{\text{Na}}^B = 2.75$ and an internal barrier of $\Delta E_{T,i}^c = 0.5 kT$. We note that the error bars were small and hence omitted. This comparison is only made for symmetrical 0.14 M solutions, and so we have predicted the current at the larger 0.4 M and 0.6 M NaCl solutions (orange and green curves respectively). **Right**, comparison of the fitted theory (full curve) with the normalised whole-cell current measured for the NaChBac mutant LDDWAD (data points) in mixed K^+/Na^+ solutions. The fitting parameters were: $\alpha = 1$, for the first ion entering (in kT) $\Delta G_{\text{Na},1}^B = 4.7$, $\Delta G_{\text{Na},2}^B = 7.3$, $\Delta G_{\text{K},1}^B = 4.5$, $\Delta G_{\text{K},2}^B = 4.8$, and for the second ion entering (in kT) $\Delta G_{\text{Na},1}^B = 8.2$, $\Delta G_{\text{Na},2}^B = 7$, $\Delta G_{\text{K},1}^B = 5.7$ and $\Delta G_{\text{K},2}^B = 3.7$. The equivalent barriers involving mixed ionic states are calculated after subtracting $kT \ln(2)$ due to the difference in permutations term W (see (1)). Finally, the internal transition barriers were (in kT): $\Delta E_{T,\text{Na}1}^c = 0.1$, $\Delta E_{T,\text{Na}2}^c = 2.8$, $\Delta E_{T,\text{K}1}^c = 1.5$ and $\Delta E_{T,\text{K}2}^c = 1.8$.

pore is unknown. Simulations estimate this parameter to take values of $\alpha \sim 0.01$ to 0.5 for pores of the widths considered [40].

In Fig. 4, we display the results of comparison with experimental recordings. In the left panel we illustrate a good fit to the single-channel $I - V$ data at a concentration of 0.14 M, and make predictions for the shape of the $I - V$ curves at larger concentrations (0.4 M and 0.6 M) and at larger voltages. We find that the pore is symmetrical with respect to voltage and calculate the energy barriers for the first and second ion entering the pore to be: $\Delta G_{\text{Na}}^B = 3.75 kT$ and $\Delta G_{\text{Na}}^B = 2.75 kT$, respectively, similar to values in [12]. The barriers decrease for the second entry, because the electrostatic attraction to the pore charge is likely to be reduced due to compensation of the total pore charge by the already present ion. Finally, we note that the diffusion coefficient takes a reasonable value with $\alpha = 0.5$, and we predict in accordance with single channel currents that saturation occurs after $\sim 0.2 \text{ V}$ [2].

In the right hand panel of Fig. 4, we consider the AMFE whole-cell experiment undertaken for the mutant (LDDWAD). For consistency in fitting we have treated the values of normalized current as values in [pA], because it is a similar order of magnitude (although different channel) to the single channel data. We are able to model the data quite accurately with the parameters given in the caption. The binding selectivity at each site ($\mathcal{S}_m = \Delta G_{\text{Na},m}^B - \Delta G_{\text{K},m}^B$) favors Na^+ over K^+ ; however, the channel is almost non-selective for the first ($m = 1$) site when adding

the first ion. The total selectivity (given by the sum over m) differs between adding the first and second ions taking the values $+2.8 kT$ and $+5.6 kT$, respectively, suggesting that it is harder for K^+ to enter if Na^+ is already occupying the pore. It is also likely that the conduction mechanism and number of binding sites will differ in this mutant in addition to protonation effects [11]; and so further analysis will be required.

4. Conclusion

In summary, we have presented a far-from-equilibrium multi-species kinetic theory explicitly tracking the permeating ions through two binding sites. It is directly related to the equilibrium statistical theory, briefly discussed here but introduced in more detail elsewhere [29, 30]; through the calculation of the transition rates and in particular their normalization.

To investigate the permeation of wild type NaChBac and a mutant we have compared the predictions of the kinetic model with two sets of experimental data (see Fig. 4). The first of these contains single-channel $I - V$ curves from which we are able to extract the effective Na^+ diffusion coefficient in the pore $D_{Na}^c \sim 6.65 \times 10^{-10} m^2 s^{-1}$, and the binding energy parameters ($\Delta G_{Na,m}^B$) of $3.75 kT$ and $2.75 kT$ for adding the first and second ions, respectively. These are identical in both sites indicating a symmetrical pore. Comparison with the second set of data (describing the mutant) enables us to recover the blocking effect AMFE. The barriers varied at each site and always remained selective to Na^+ , although this selectivity was small in the first ($m = 1$) site when adding the first ion.

In future, we aim to further compare NaChBac and its mutants by extension of the number of binding sites, analysis of the effects of mixed-valence i.e., Na^+/Ca^{++} and the effects of changing the structure. The enhanced conduction behavior observed within the kinetic theory is also a topic for further research. Finally, we comment that we expect our model to be applicable to the permeation of other voltage-gated ion channels and artificial nanopores.

Acknowledgments

We are grateful to Bob Eisenberg, Igor Kaufman, Igor Khovanov, Aneta Stefanovska and Adam Parker for helpful discussions. The work was funded by a Leverhulme Trust Research Project Grant RPG-2017-134 and by the Engineering and Physical Sciences Research Council under Grant No. EP/M015831/1.

References

- [1] J. Zheng and M. Trudeau (eds.), *Handbook of Ion Channels* (CRC Press Taylor & Francis Group, Boca Raton, 2015).
- [2] B. Hille, *Ion Channels Of Excitable Membranes*, 3rd edn. (Sinauer Associates, Sunderland, MA, 2001).

W. A. T. Gibby *et al.*

- [3] F. Ashcroft, *Ion Channels and Disease* (Academic press, 1999).
- [4] F. Ashcroft, From molecule to malady, *Nature* **440** (2006) 440–447.
- [5] D. Ren, B. Navarro, H. Xu, L. Yue, Q. Shi and D. Clapham, A prokaryotic voltage-gated sodium channel, *Science* **294** (2001) 2372–2375.
- [6] D. Gillespie and D. Boda, The anomalous mole fraction effect in calcium channels: A measure of preferential selectivity, *Biophys. J.* **95** (2008) 2658–2672.
- [7] W. Nonner, D. P. Chen and B. Eisenberg, Anomalous mole fraction effect, electrostatics, and binding in ionic channels, *Biophys. J.* **74** (1998) 2327–2334.
- [8] L. Heginbotham and R. MacKinnon, Conduction properties of the cloned Shaker K⁺ channel, *Biophys. J.* **65** (1993) 2089–2096.
- [9] S. Ye, Y. Li and Y. Jiang, Novel insights into K⁺ selectivity from high-resolution structures of an open K⁺ channel pore, *Nat. Struct. Mol. Biol.* **17** (2010) 1019.
- [10] W. Almers, E. McCleskey and P. Palade, A non-selective cation conductance in frog muscle membrane blocked by micromolar external calcium ions, *J. Chem. Phys.* **353** (1984) 565–583.
- [11] O. Fedorenko, I. K. Kaufman, W. A. T. Gibby, D. Luchinsky, S. K. Roberts and P. V. E. McClintock, Quantized dehydration and the determinants of selectivity in the NaChBac bacterial sodium channel, arXiv:1803.07063.
- [12] C. Guardiani, P. Rodger, O. Fedorenko, S. Roberts and I. Khovanov, Sodium binding sites and permeation mechanism in the NaChBac channel: A molecular dynamics study, *J. Chem. Theor. Comp.* (2016) arXiv:10.1021/acs.jctc.6b01035.
- [13] C. Guardiani, O. A. Fedorenko, S. K. Roberts and I. A. Khovanov, On the selectivity of the NaChBac channel: An integrated computational and experimental analysis of sodium and calcium permeation, *Phys. Chem. Chem. Phys.* **19** (2017) 29840–29854.
- [14] E. F. Pettersen, T. D. Goddard, C. C. Huang, G. S. Couch, D. M. Greenblatt, E. C. Meng and T. E. Ferrin, UCSF Chimera — A visualization system for exploratory research and analysis, *J. Comput. Chem.* **25** (2004) 1605–1612.
- [15] P. Nelson, A permeation theory for single-file ion channels: One- and two-step models, *J. Chem. Phys.* **134** (2011) 165102–165114.
- [16] S. Agah, M. Pasquali and A. Kolomeisky, Theoretical analysis of selectivity mechanisms in molecular transport through channels and nanopores, *J. Chem. Phys.* **142** (2015) 044705.
- [17] B. Hille, Ionic selectivity, saturation, and block in sodium channels. A four-barrier model, *J. Gen. Physiol.* **66** (1975) 535–560.
- [18] E. Kitzing, A novel model for saturation of ion conductivity in transmembrane channels, in *Membrane Proteins: Structures, Interactions and Models: Proc. Twenty-Fifth Jerusalem Symp. Quantum Chemistry and Biochemistry Held in Jerusalem, Israel, May 18-21, 1992*, eds. A. Pullman, J. Jortner and B. Pullman (Springer Netherlands, Dordrecht, 1992), pp. 297–314.
- [19] W. R. Bauer and W. Nadler, Cooperative transport in nanochannels, *Phys. Rev. E* **88** (2013) 010703.
- [20] A. M. Berezhkovskii and S. M. Bezrukov, Mapping intrachannel diffusive dynamics of interacting molecules onto a two-site model: Crossover in flux concentration dependence, *J. Phys. Chem. B* **122** (2018) 10996–11001.
- [21] M. Grabe, D. Bichet, X. Qian, Y. N. Jan and L. Y. Jan, K⁺ channel selectivity depends on kinetic as well as thermodynamic factors, *Proc. Natl. Acad. Sci. USA* **103** (2006) 14361–14366.
- [22] B. Eisenberg, *Crowded Charges in Ion Channels* (Wiley-Blackwell, 2011), pp. 77–223.
- [23] K. Cooper, P. Gates and R. Eisenberg, Diffusion theory and discrete rate constants in ion permeation, *J. Membr. Biol.* **106** (1988) 95–105.

- [24] P. Hänggi, P. Talkner and M. Borkovec, Reaction-rate theory: Fifty years after Kramers, *Rev. Mod. Phys.* **62** (1990) 251.
- [25] W. Nonner, D. P. Chen and B. Eisenberg, Progress and prospects in permeation, *J. Gen. Physiol.* **113** (1999) 773–782.
- [26] E. Abad, J. Reingruber and M. Sansom, On a novel rate theory for transport in narrow ion channels and its application to the study of flux optimization via geometric effects, *J. Chem. Phys.* **130** (2009) 02B608.
- [27] C. Gardiner, *Handbook of Stochastic Methods: For Physics, Chemistry and the Natural Sciences* (Springer, Berlin, 2002).
- [28] F. Skinner, C. Ward and B. Bardakjian, Permeation in ionic channels: A statistical rate theory approach, *Biophys. J* **65** (1993) 618–629.
- [29] D. G. Luchinsky, W. A. T. Gibby, I. Kaufman, D. A. Timucin and P. V. E. McClintock, Statistical theory of selectivity and conductivity in biological channels, arXiv: 1604.05758.
- [30] D. G. Luchinsky, W. A. T. Gibby, I. K. Kaufman, P. V. E. McClintock and D. A. Timucin, Relation between selectivity and conductivity in narrow ion channels, in *2017 Int. Conf. Noise and Fluctuations (ICNF)* (Vilnius, Lithuania, 2017), pp. 1–4.
- [31] D. Gillespie, W. Nonner, D. Henderson and R. S. Eisenberg, A physical mechanism for large-ion selectivity of ion channels, *Phys. Chem. Chem. Phys.* **4** (2002) 4763–4769.
- [32] B. Roux, T. Allen, S. Berneche and W. Im, Theoretical and computational models of biological ion channels, *Quart. Rev. Biophys.* **37** (2004) 15–103.
- [33] Y. Alhassid, Statistical theory of quantum dots, *Rev. Mod. Phys.* **72** (2000) 895–968.
- [34] C. Beenakker, Theory of Coulomb-blockade oscillations in the conductance of a quantum dot, *Phys. Rev. B* **44** (1991) 1646–1656.
- [35] B. Roux, Statistical mechanical equilibrium theory of selective ion channels, *Biophys. J.* **77** (1999) 139–153.
- [36] W. Im, S. Seefeld and B. Roux, A grand canonical Monte Carlo Brownian dynamics algorithm for simulating ion channels, *Biophys. J.* **79** (2000) 788–801.
- [37] J. Zhang, A. Kamenev and B. I. Shklovskii, Conductance of ion channels and nanopores with charged walls: A toy model, *Phys. Rev. Lett.* **95** (2005) 148101.
- [38] J. Zhang, A. Kamenev and B. I. Shklovskii, Ion exchange phase transitions in water-filled channels with charged walls, *Phys. Rev. E* **73** (2006) 051205.
- [39] I. Kaufman, P. McClintock and R. Eisenberg, Coulomb blockade model of permeation and selectivity in biological ion channels, *New J. Phys.* **17** (2015) 083021.
- [40] D. P. Tieleman, P. C. Biggin, G. R. Smith and M. S. P. Sansom, Simulation approaches to ion channel structure-function relationships, *Quart. Rev. Biophys.* **34** (2001) 473–561.